Article

Discovery Medicine 2026; 38(206): 877–891
https://doi.org/10.24976/Discov.Med.202638206.72

Multi-Omics Reveals the Associations Among the Gut Microbiota, Glycerophospholipid Metabolism, and Reduced Autophagy in Sepsis-Associated Encephalopathy

Yan Li[1,2,3,4], Zhenzhen Qu[2,3,4], Aoxuan Zhen[5,6], Qingsheng Huang[1], Qi Qiao[2,3,4], Hongyu Li[1], Yu Zhao[1], Qi Zhang[1], Wei Zhou[5,6,*], Weiping Wang[2,3,4,*]

[1]Department of Critical Care Medicine, The Third Hospital of Hebei Medical University, 050000 Shijiazhuang, Hebei, China
[2]Key Laboratory of Clinical Neurology, Ministry of Education, Hebei Medical University, 050000 Shijiazhuang, Hebei, China
[3]Department of Neurology, The Second Hospital of Hebei Medical University, 050000 Shijiazhuang, Hebei, China
[4]Key Neurological Laboratory of Hebei Province, 050000 Shijiazhuang, Hebei, China
[5]Hebei Food Safety Key Laboratory, Hebei Engineering Research Center for Special Food Safety and Health, Hebei Food Inspection and Research Institute, 050227 Shijiazhuang, Hebei, China
[6]Key Laboratory of Special Food Supervision Technology, State Administration for Market Regulation, 050227 Shijiazhuang, Hebei, China
*Correspondence: zhouwei@nepp.com.cn (Wei Zhou); wangweiping@hebmu.edu.cn (Weiping Wang)
Submitted: 10 November 2025 Revised: 4 February 2026 Accepted: 2 March 2026 Published: 20 March 2026

Background: Sepsis-associated encephalopathy (SAE) is defined by neurological impairment resulting from systemic infections. The gut microbiota has been shown to affect the brain via the gut–brain axis (GBA) in SAE. However, the underlying molecular mechanisms are unclear. This research focused on examining the potential mechanisms by which the gut microbiota and the GBA are involved in SAE by integrating multi-omics data.

Methods: An SAE model was established using 7–8-week-old male rats via lipopolysaccharide (LPS) injection combined with caecal ligation and puncture (CLP). The gut microbiota (via 16S rRNA sequencing) and metabolomes were profiled to analyze variations in gut microbiota composition and metabolite abundance in the faeces and hippocampus. Western blot and RT-qPCR analyses were applied to measure the expression of proteins or genes associated with autophagy in the hippocampus.

Results: SAE rat models presented significant differences in gut microbiota composition, characterized by reduced abundances of the genera Butyricimonas, Muribaculaceae, and Bacteroides and increased abundance of the genera Aeromonas and Family_XIII_UCG-00. Integrated analysis of untargeted metabolomics data for the faeces and metabolomics data for the hippocampus revealed that glycerophospholipid metabolism was altered in both the faeces and hippocampus in SAE rat models. Molecular analyses revealed that the activity of hippocampal autophagy pathways was reduced in SAE rat models, in contrast with rats in the non-SAE group and the control group.

Conclusion: Combining multi-omics data with molecular analysis data revealed a potential association among the gut microbiota, host glycerophospholipid metabolism and reduced neuronal autophagy in SAE model rats. The study contributes to a better understanding of the gut microbiota's involvement in SAE.

Keywords: sepsis-associated encephalopathy; gut microbiota; glycerophospholipid metabolism; autophagy

Introduction

Sepsis is a complicated disorder characterized by life-threatening organ failure due to an unbalanced immune response to infection [1]. Sepsis usually impairs multiple organ functions, influences the immune, hematopoietic, and nervous systems [2]. Sepsis-associated encephalopathy (SAE) is marked by sudden cognitive decline due to systemic peripheral infections, affecting as many as 70% septic patients [3,4]. SAE is associated with increased mortality rates in ICU patients and adversely influences the quality of life among survivors, imposing a substantial financial burden due to neurological sequelae such as residual cognitive dysfunction and disturbances of consciousness ranging from mild delirium to coma [5,6].

The mechanisms underlying SAE pathophysiology involve oxidative stress, activation of microglia and astrocytes, elevation of inflammation levels, mitochondrial dysfunction, neuronal death, alteration of blood–brain barrier permeability, and other detrimental metabolic changes [7–10]. According to a recent review, multiple pathways, including ferroptosis, pyroptosis, and autophagy, are associated with the progression of SAE [11]. A previous study demonstrated that regulating the level of astrocyte

autophagy can reduce neuronal damage and cognitive dysfunction in SAE [12]. However, owing to the presence of blood-brain barrier (BBB), the brain is isolated from the peripheral system and possesses immune privilege. During sepsis, the precise mechanism by which peripheral infections lead to acute brain injury remains unclear. In critical illnesses, the gut is critically involved in the pathophysiology of sepsis, particularly in the development of multiple organ dysfunction syndrome. Sepsis induced gut dysfunction exacerbates systemic inflammation, provoking damage in distant organs through the gut-organ axis [13].

The gut microbiota and microbial metabolites participate in the pathophysiology of SAE through the gut–brain axis (GBA) [14,15]. Although gut dysbiosis can promote SAE via the GBA, the gut microbiota and its metabolites do not directly target the central nervous system (CNS) due to the protective roles of the intestinal barrier and the BBB [5,16]. Instead, their interaction with the brain is mediated predominantly by immune, neural, endocrine, and metabolic signalling pathways [17,18]. Lipopolysaccharide (LPS) activates intestinal immunity by triggering the TLR4/NF-κB pathway, thereby disrupting the intestinal epithelium and the BBB. Subsequently, it traverses the BBB to directly impact the CNS [19,20]. Additionally, short-chain fatty acids (SCFAs), principal microbial metabolites, exert neuroprotective effects through dual mechanisms: they suppress peripheral inflammation via free fatty acid receptor 2 (FFAR2) and sustain the microglial M2 phenotype [21,22]. Moreover, the microbe- derived metabolite indole-3-propionic acid acts as a neuroprotective agent by exerting an anti-inflammatory effect and has shown to protect against SAE in mice [23].

Studies have shown that the bidirectional gut-brain communication contributes significantly to the pathogenesis and progression of SAE [23,24]. However, the mechanism by which the GBA participates in SAE remains incompletely understood. This study investigates how the gut microbiota contributes to SAE via the GBA, utilizing an integrated multi-omics approach. 16S rRNA sequencing and metabolomics were used to analyze alterations in gut microbial community structure and metabolite profiles in both faecal and hippocampal samples. We further examined the expression of key autophagy-related proteins and genes in the hippocampus using Western blott and RT-qPCR analyses. Then, we integrated 16S rRNA gene sequencing, metabolomics, and molecular analysis data to characterize cerebral alterations and identify associated factors in SAE rats. This study offers direct evidence for elucidating the role of GBA in SAE.

Materials and Methods

Experimental Animals

A total of 60 male specific pathogen-free (SPF)-grade rats, aged 6–7 weeks and weighing 200 $\pm$ 20 g, were obtained from Beijing Vito Bio-Tech Co., Ltd. (license number 9003144). All animal procedures were approved by the institutional ethics committee and conducted in compliance with guidelines for laboratory animal care. Under standardized conditions (22 $\pm$ 2 °C, 55 $\pm$ 5% humidity, 12-h light/dark cycle), rats were housed in individually ventilated cages (2–3 animals per cage) with free access to food and water. The rats were acclimatized to the experimental conditions for one week before the experiments. The experimental procedures were conducted under approval by the Institutional Animal Care and Use Committee (IACUC) of The Second Hospital of Hebei Medical University (ethics number: 2023–AE322).

SAE Model

Randomization via a random number table was employed to assign animals to two experimental groups at a 3:1 ratio: sepsis group and sham-operated controls (sham group). Sepsis group rats were categorized into an SAE group and a non-SAE (NSAE) group based on standard SAE diagnostic criteria [25,26]. Subsequently, the SAE cohort was subdivided into an untreated subgroup (SAENA) and a microbiota-inhibited subgroup (SAEA) using a random number table. The SAEA group rats received an enema containing an antibiotic mixture daily for 3 days. The antibiotic mixture included vancomycin (100 mg/kg), neomycin sulphate (200 mg/kg), metronidazole (200 mg/kg), and ampicillin (200 mg/kg) (vancomycin, V8050, Solarbio. Beijing, China; neomycin sulfate 10 g/L, N8090, Solarbio. Beijing, China; metronidazole 1 g/L, M8060 Solarbio, Beijing, China; ampicillin 5 g/L, A6920, Solarbio, Beijing, China). The rats in the SAENA group were administered an equal volume of saline via oral gavage. Three days after modelling, all rats in the sham, NSAE and SAE groups were then euthanised in two batches. Some rats underwent transcranial perfusion following intraperitoneal injection of pentobarbital sodium at a dose of 40 mg/kg three days following the establishment of the animal model, while others received intraperitoneal injection of pentobarbital sodium at a dose of 100 mg/kg after isoflurane anesthesia, induced at 3%–4% concentration in oxygen (1–2 L/min) until loss of righting and corneal reflexes, then maintained at 2%–2.5% (0.5–1 L/min) until complete cessation of spontaneous respiration and cardiac activity.

According to Siami's study [25], the diagnostic criteria for SAE include a decrease in neurological and behavioural scores and an increase in theta waves under electroencephalographic (EEG) monitoring, or a significant decrease in the amplitude of P1 in evoked potentials, as well as a significant prolongation of the latencies of S-P1 and N-P1 [26].

As previously described [27], SAE was induced in rats by a combination of cecal ligation and puncture (CLP) and intraperitoneal lipopolysaccharide injection (LPS, GC205009, Servicebio, Wuhan, China Seville

Biotechnology Co., Ltd.). In brief, the rats were administered LPS (5 mg/kg) via intraperitoneal injection, followed by CLP surgery the next day. According to the CLP protocol by José C *et al*. [27], rats were anesthetized by intraperitoneal injection of pentobarbital sodium (40 mg/Kg) and were subsequently maintained in a supine position on the operating platform. Next, a midline abdominal incision (approximately 2 cm) was created to access the cecal region. The mesentery and caecum were then separated, and the caecum was ligated 3 cm distal to the ileocecal valve. The caecum was then gently subjected to two punctures using a 22-gauge needle and lightly compressed to allow faecal debris to flow into the peritoneal cavity. Sham group rats received the same surgical intervention as the model group, excluding the CLP procedure. All the rats were injected with physiological saline (5 mL/100 g) for fluid resuscitation.

Neurobehavioural Evaluation

Neurobehavioural evaluations were performed at 12 hours and 24 hours after modelling. Neurological function in rats was quantitatively assessed based on a series of reflexes: auricular, corneal, righting, tail-flick, and escape. The auricular reflex was elicited by gentle stimulation of the external auditory canal and observing whether the head rotated forcefully. A positive corneal reflex, indicated by a blinking or head-shaking response, was recorded following gentle stimulation of the cornea with a cotton swab. We tested the righting reflex by placing the rat supine; a normal response was the animal promptly righting itself into a prone position with full extension of all limbs. The tail-flick and escape reflexes were assessed by briefly stimulating the tail, which should trigger a response of avoidance or head turning to evade the noxious stimulus.

The composite neurological score was derived from the summation of these five reflex scores, using the criteria below: 0: absence of reflex, 1: diminished reflex (lack of reflex within 10 seconds), 2: normal reflex. The total possible score for each was 2 points, yielding a maximum total score of 10 points.

Surgical Implantation of Electrodes and Video-Electroencephalogram (vEEG) Monitoring

One week before CLP procedure, epidural EEG electrodes were surgically implanted in anesthetized rats. Briefly, rats were anesthetized via intraperitoneal injection of pentobarbital sodium (40 mg/Kg), and secured in a stereotaxic frame (RWD, 68809, Shenzhen, China). Recording electrodes (0.6 mm stainless steel screws) were then implanted 2.5 mm posterior to the fontanel and 2.5 mm lateral to the right sagittal suture. The reference and ground electrodes were symmetrically positioned on the contralateral side, respectively. A flexible wire was used to attach the electrodes to a microconnector, which was fixed with dental acrylic. After one week of post-operative recovery, the rats were individually housed in acrylic cages and interfaced with an amplifier (Warner Instruments, dp304, USA). Continuous vEEG was then recorded for up to 3 days using a Power Lab 8/35 system after modelling (AD Instruments, Colorado Springs, CO, USA) for signal digitization and acquisition.

Perfusion Fixation and Brain Histopathology

After completion of the neurobehavioural tests and EEG recording, the rats were anaesthetized by intraperitoneal injection of pentobarbital sodium (40 mg/Kg) and euthanized by transcranial perfusion, initially with ice-cold saline, followed by 4% paraformaldehyde (PFA) (Servicebio, G1005, Wuhan, China) prepared in 0.1 M phosphate-buffered saline (PBS). Following extraction, the brains underwent precise dissection of the frontal lobe and hippocampus. Following 24-hour fixation in 4% PFA at 4 °C, the tissue samples underwent dehydration, clearing, and paraffin embedding; 4-µm-thick serial sections were prepared. Haematoxylin–eosin (HE) staining of coronal sections (encompassing the complete hippocampus) and cortical tissues collected from 2 mm and 7 mm posterior to bregma was performed to assess inflammatory changes in the cerebral cortex and hippocampus. The HE-stained sections (three sections per animal) were examined at 400× magnification using an Olympus BX51 light microscope (Tokyo, Japan).

16S rDNA Sequencing

Faecal samples collected from rat colons were snap-frozen at –80 °C for subsequent microbial DNA extraction, which was performed using the MagPureSoil DNA LQ Kit. (Magan, M5635-02, USA). Amplification of the V3-V4 hypervariable regions of the 16S rRNA gene was performed employing the universal primers 343F (5′-TACGGRAGGCAGCAG-3′) and 798R (5′-AGGGTATCTAATCCT-3′) for bacterial diversity analysis. Following the manufacturer's instructions, sequencing was conducted on the Illumina NovaSeq 6000 platform (Illumina NovaSeq, USA). Bioinformatics analyses were performed with QIIME 2.0 (2020.11, USA), and alpha diversity was evaluated using four indices: Shannon, Simpson, Chao, and ACE. 16S rRNA gene amplicon sequencing and subsequent bioinformatic analysis were conducted using OE Biotech Co., Ltd. (Shanghai, China). The library construction, sequencing, and bioinformatic analysis methods are provided in **Supplementary Material 1**.

LC–MS/MS Analysis of Faeces

Following thawing of the –80 °C preserved faecal samples, 30 mg of each sample was transferred to a 1.5 mL centrifuge tube. Two small steel beads and 600 µL of a methanol-water mixture (4:1, v/v) containing a mixed internal standard at 4 µg/mL were added. The samples were precooled at –40 °C for 2 minutes and homogenized using

a grinder (60 Hz, 2 min) (Wonbio-E, Wonbio, Shanghai, China). The samples were subjected to ice-bath sonication for 10 min for extraction and then incubated at –40 °C. After centrifugation at 13,000 rpm and 4 °C for 10 minutes, 150 µL of supernatant was harvested and filtered through a 0.22 µm organic solvent-resistant membrane, transferred to LC vials, and stored at –80 °C until LC-MS analysis. For quality control (QC), pooled samples were prepared by combining aliquots from each experimental sample. All extraction reagents were pre-cooled at –20 °C pre-use.

The Metabolomic profiling was conducted using Shanghai Luming Biological Technology Co., Ltd. (Shanghai, China). All related methodologies for chromatography and LC–MS/MS procedures, conditions, and data processing methods are documented in **Supplementary Material 2**.

LC–MS/MS Analysis of Hippocampal Samples

Hippocampal specimens preserved at –80 °C were equilibrated to room temperature prior to processing. A 30 mg aliquot of each hippocampal specimen was weighed into an Eppendorf tube (1.5 mL), which contained 400 µL of a standardized internal reference solution (L-2-chlorophenylalanine at 4 µg/mL in methanol). Metabolic profiling was conducted on a Waters ACQUITY UPLC I-Class PLUS system coupled with a Thermo Scientific Q Exactive mass spectrometer (HESI source) using ACQUITY UPLC HSS T3 columns (1.8 µm, 2.1 × 100 mm), with data collection performed in dual-polarity modes (positive/negative). The metabolomic data analysis methods are documented in **Supplementary Material 2**.

The metabolomic data were analysed by Shanghai Luming Biological Technology Co., Ltd. (Shanghai, China).

Western Blot Analysis

The homogenized hippocampal samples from rats were combined with RIPA lysis buffer (Biosharp, Cat. No. BL504A) and then subjected the mixture to centrifugation (12,000 ×g, 10 min, 4 °C). The protein concentration of the collected supernatant was determined using a BCA protein assay kit (Biosharp, China, Cat. No. BL521S). The Protein separation were subsequently resolved by 10% sodium dodecyl sulphate-polyacrylamide gel electrophoresis (SDS–PAGE) on a DYY-6D apparatus (Beijing Liuyi Biotechnology, China). Subsequent to electrophoresis, we transferred the proteins onto a PVDF membrane (Merck Millipore, IPVH00010), then blocked using 5% BSA for 1 h at ambient temperature. The membrane was then treated with the designated primary antibodies, including an anti-mTOR antibody (Invitrogen, UK, Cat. No. MA5-41124), an anti-phospho-mTOR (Invitrogen, UK, Cat. No. 44-1125G), an anti-β-actin antibody (Sigma–Aldrich, USA, Cat. No. A5441), and an anti-LC3 antibody (Abcam, USA, Cat. No. ab48394), with nocturnal incubation at 4 °C. Following removal of the unbound primary antibodies, the membrane was subsequently probed with the matching secondary antibody, anti-rabbit IgG (H+L) (Thermo Scientific, USA, Cat. No. 31460) or anti-mouse IgG (H+L) (Thermo Scientific, USA, Cat. No. 31430) and secondary antibodies, under room temperature conditions for 60 minutes. The membrane was then imaged via a ChemiDoc™ MP imaging system (Bio-Rad, USA), and the bands were detected with a high-sensitivity ECL chemiluminescent detection kit (SEVEN, China, Cat. No. SW181-02).

Real-Time Quantitative Reverse Transcription–PCR (qRT–PCR) Analysis

To quantify the expression of target genes, qRT-PCR analysis was conducted. Following the collection and storage of hippocampal tissues from rats at –80 °C, we proceeded to extract total RNA with TRNzol Universal Reagent (Tiangen, Y1613) and generated cDNA with the FastKing cDNA Synthesis Kit (with gDNase) (Tiangen, China, Cat. No. Y1609). qPCR was performed using the Talent qPCR PreMix (SYBR Green) Kit (Tiangen, China, Cat. No. FP209) on a Quant Studio 5 Real-Time PCR System (Thermo Fisher Scientific, USA), was initiated with a denaturation phase (95 °C for 3 min), and then underwent 40 thermal cycles of 95 °C for 5 s, 60 °C for 10 s, and 72 °C for 15 s. The primer sequences employed in this study are listed below: GAPDH, forward primer: 5′-TGCACCACCAACTGCTTAGC-3′, reverse primer: 5′-GGCATGGACTGTGGTCATGAG-3′; ATG5, forward primer: 5′-TGAAGGAAGTTGTCTGGATAGCTCA-3′, reverse primer: 5′-AAGTCTGTCCTTCCGCAGTC-3′; Beclin 1, forward primer: 5′-GCACGCCATGTATAGCAAAGA-3′, reverse primer: 5′-GGAAGAGGGAAAGGACAGCAT-3′; IL-6, forward primer: 5′-AGTTGCCTTCTTGGGACTGATGT-3′, reverse primer: 5′-GGTCTGTTGTGGGTGGTATCCTC-3′; and Caspase 3, forward primer: 5′-CGATTATGCAGCAGCCTCAA-3′, reverse primer: 5′-AGGAGATGCCACCTCTCCTT-3′. Gene expression was normalized to the endogenous control GAPDH and further standardized against the reference value in the control group, with relative expression calculated using the $2^{-\Delta\Delta C_t}$ method.

Statistical Analysis

All quantitative data are presented as the mean ± standard deviation (SD) and data normality was assessed using the Shapiro Wilk test before further analysis. Depending on data distribution normality, two-group comparisons utilized either the unpaired *t*-test (normal data) or Mann-Whitney U test (non-normal data), as appropriate. Survival outcomes were analyzed using the Kaplan-Meier method, with intergroup comparisons performed via the log-rank test. Comparisons across multiple groups were conducted using analysis of variance (ANOVA) and LSD test. For

the ANOVA testing, post-hoc analysis was performed. To identify differential species among different groups, the Kruskal-Wallis test was employed to analyze differential bacterial species across groups when the data did not conform to a normal distribution. Associations between gut microbiota and metabolites (from faeces and brain) were determined by Spearman correlation, followed by Benjamini-Hochberg FDR correction. Data analysis was performed using R version 4.3.1 (The R Foundation for Statistical Computing, Vienna, Austria. Website: https://www.R-project.org/foundation/). A significance threshold of $p < 0.05$ was applied to all post hoc tests.

Results

Establishment of the SAE Model

To determine the underlying mechanisms by which the gut microbiota is involved in SAE, the SAE model was first assessed by neurobehavioural evaluation, vEEG and brain histopathology. A total of 60 rats were included in this experiment; following brain electrode implantation, three rats succumbed to death within 72 hours and 57 surviving rats were randomly divided into the sepsis group and the sham group (SH) at a 3:1 ratio using a random number table (sham group, n = 14; sepsis group, n = 43). The rats in the sepsis group manifested as curling, shivering, reduced activity, and rapid breathing after LPS injection combined with CLP. Within 24 hours after modelling, 26 rats developed SAE, and 17 rats were defined as the non-SAE (NSAE) group, resulting in an overall SAE incidence rate of 60.5% (26/43). 26 Rats in the SAE cohort were further subdivided into two subgroups: an untreated SAE subgroup (SAENA, n = 18) and a microbiota-inhibited SAE subgroup (SAEA, n = 8). Subsequently, 10 rats in the SAENA group were subjected to Haematoxylin–eosin (HE) staining and molecular biological assays three days following the establishment of the animal model. Within 72 hours after modelling, 18 rats died (sham group (n = 2) and sepsis group (n = 16)). Survival outcomes were assessed 3 days following the establishment of the sepsis model, including the rats allocated for HE and molecular biological assays. Statistical analyses of survival outcomes demonstrated distinct intergroup differences. The survival time of rats in the SAE group was statistically significantly shorter than that in the Sham group ($p < 0.05$), whereas that in the NSAE group was longer than that in the SAE group ($p < 0.05$). Furthermore, no statistically significant difference was observed in the survival time between the NSAE group and the SH group ($p > 0.05$). In addition, the SAEA group exhibited a statistically significant prolongation of survival time compared with the SAENA group ($p < 0.05$) (Fig. 1A).

From recovery from anaesthesia up to 24 hours after surgery, the neurological scores of the rats in the SH group remained within the normal range. Rats in the SAE groups and the NSAE groups exhibited significantly reduced neurological scores compared to those in the SH group. The mean total neurological scores of the SAE, NSAE and SH groups were 8.3, 5.8 and 10, respectively. Significant differences were detected among the three groups ($p < 0.05$) (Fig. 1B).

To evaluate the SAE modelling, a continuous vEEG monitoring system was employed to monitor the EEG activity in each group from 1 week before to 3 days after modelling. A comparison of the EEG results between the SAE group and the NSAE group revealed that the background EEG activity in the SAE group was slower (Fig. 1C–E). EEG activity of the SAE rats was manifested as a rhythm dominated by δ waves (0.2–3.5 Hz), accompanied by periodic discharges, along with low voltage and suppression patterns, as shown in Fig. 1E.

Under light microscopy, neurons and glial cells in the cortical and hippocampal regions of rats in the sham operation group presented a normal morphology with clear cellular structures. In the NSAE group, some neurons and glial cells located in the cortex and hippocampus exhibited morphological changes with unclear cellular structures. However, there were no obvious neuronal pyknosis or vascular changes. In the SAE group, obvious neuronal pyknosis and hyperchromatism, nuclear condensation, unclear cellular structures, enlarged perineuronal spaces, and enlarged perivascular spaces around glial cells and blood vessels were observed in both the hippocampus and cortex (Fig. 1F).

Analysis of the Gut Microbiota

To delineate the differences in gut microbiota abundance among the SAENA, SAEA, NSAE, and SH groups, 16S rRNA gene sequencing was performed on collected fecal specimens. Shannon and Ace indices were calculated to evaluate the α-diversity in various groups. There was a significant difference between SAE and SH mice with respect to α-diversity (Fig. 2A,B). Analysis of α-diversity revealed significant differences in the Shannon index between the SAENA and SH groups ($p < 0.05$) (Fig. 2C). A significant difference in α-diversity of gut microbiota was observed based on the Shannon index among the SAEA, SAE, and SH groups ($p < 0.05$) (Fig. 2D). PCA data showed distinctive microbial communities in the fecal microbiota between the SAE and SH groups ($p < 0.05$) (Fig. 2E). Analysis of β diversity using PCoA indicated a statistically significant difference among the SAENA, NSAE, and SH groups ($p < 0.05$) (Fig. 2F). A significant difference in β diversity was demonstrated through PCoA among the SAEA, SAENA, and SH groups ($p < 0.05$) (Fig. 2G). Furthermore, among these groups, we analyzed compositional features of gut microbiota from phylum to genus level. There was no significant difference in the phylum-level composition of the gut microbiota among the SAENA, NSAE, and SH groups ($p > 0.05$) (Fig. 2H). However, a significant difference in genus- level composition of the gut microbiota was detected

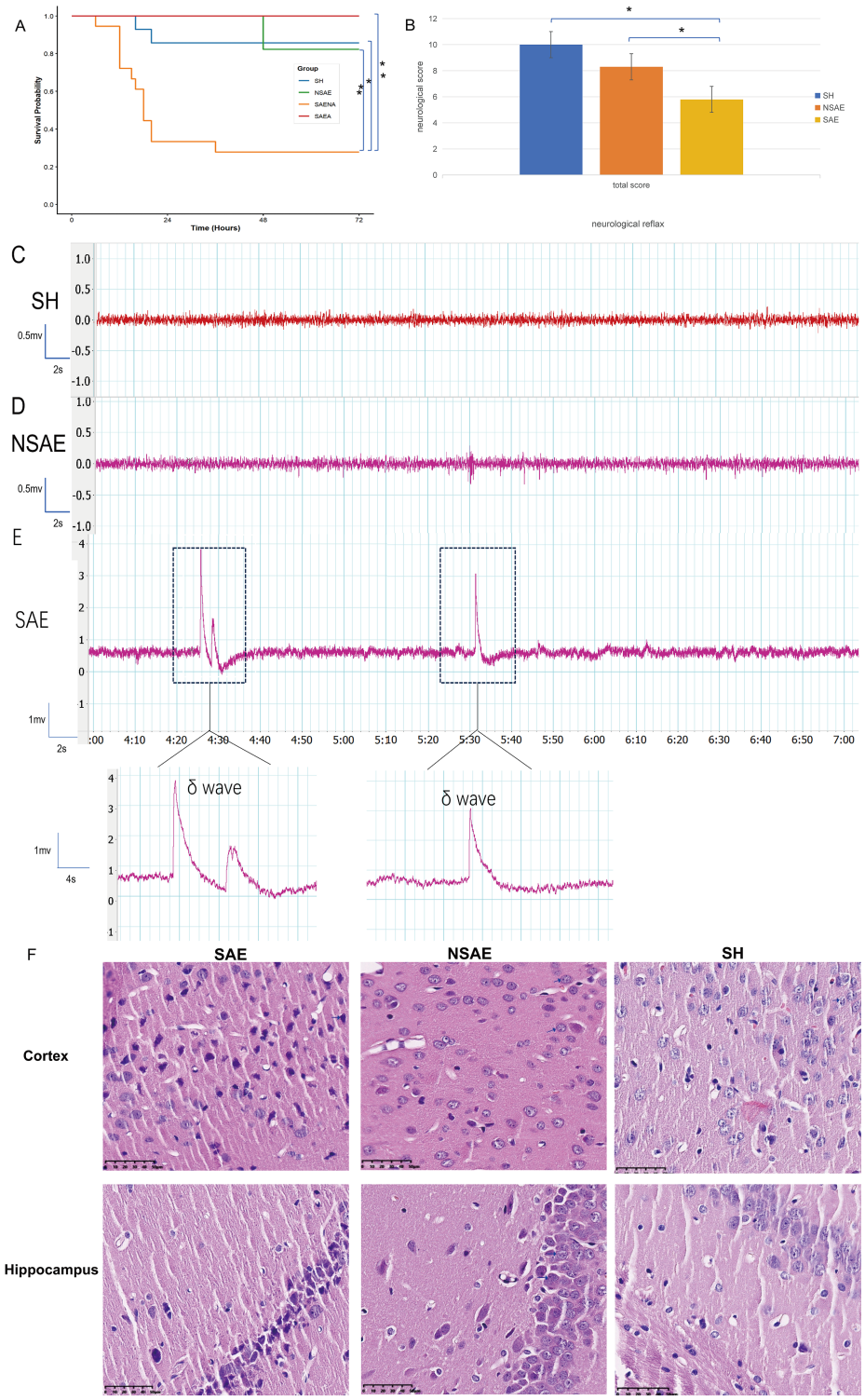

Fig. 1. Neurological function evaluation, Survival Curves, Microscopic images and EEG among the different groups. (A) Statistical Comparison of Survival Curves across the Experimental Groups (n = 57). (B) Comparisons of neurological scores among the different groups (n = 43). (C–E) EEG signals from the SH, NSAE, and SAE groups (continuous vEEG monitoring, Power Lab 8/35 system). The characteristic regions of the EEG in the SAE group were marked with a dashed line (n = 6, per group). (F) Representative images of HE-stained sections of the cortex and hippocampus (light microscope (Olympus BX51, Tokyo, Japan)), n = 6 per group. Scale bar = 50 µm (HE×400). (*$p < 0.05$, **$p < 0.01$). SAE, sepsis-associated encephalopathy; NSAE, non-sepsis-associated encephalopathy; SAENA, sepsis-associated encephalopathy without antibiotic treatment; SAEA, sepsis-associated encephalopathy with antibiotic treatment; SH, sham group; EEG, electroencephalographic; vEEG, video-electroencephalogram; HE, Haematoxylin–eosin.

among the three groups ($p < 0.05$) (Fig. 2I). The SAE group exhibited significantly decreased abundances of Muribaculaceae, Bacteroides, Butyricimonas, and Holdemania versus the SH group ($p < 0.05$) (Fig. 2J–M). In contrast, the abundances of Aeromonas increased in the SAENA group than in the NSAE group ($p < 0.05$) (Fig. 2N), the abundances of [Bacteroides] _pectinophilus_ group increased in the SAENA group than in the NSAE and SH group ($p < 0.05$) (Fig. 2O), and the abundances of Family_XIII_UCG-001 increased in the SAENA group than in the SH group ($p < 0.05$) (Fig. 2P). The abundances of *Prevotella, Muribaculaceae*, and *Bacteroides* decreased in the SAEA group versus the SAENA group and the SH group ($p < 0.05$) (Fig. 2Q,R,T). *Butyricimonas* and *Prevotella* were decreased both in the SAEA and SAENA groups versus the SH group ($p < 0.05$) (Fig. 2S). In contrast to the SH and SAENA groups, the abundances of Escherichia and Shigella increased in the SAEA group ($p < 0.05$) (Fig. 2U). The abundances of Morganella were increased in the SAEA group versus the SAENA group ($p < 0.05$) (Fig. 2V). LEfSe analysis demonstrated that the dominant genera in the SAENA group included Aeromonas, Family_ XIII_UCG-001, [Bacteroides]_pectinophilus_group and Butyricicoccus ($p < 0.05$) (Fig. 2W). The differentially enriched gut microbes were associated with key pathways, including flavonoids biosynthesisand linolenic acid metabolism. The metabolism of flavonoids and linoleic acid was significantly decreased in rats with SAE ($p < 0.05$) (Fig. 2X).

Metabolomic Analysis of the Faeces and Hippocampal Tissues

Analysis of Metabolites With Different Abundance in Feces Samples and Associated Metabolic Pathways

To further explore differentially abundant metabolites among SAE rats, NSAE rats and SH rats, untargeted metabolomics was employed to identify metabolic changes in gut feces and brain tissue, respectively. PLS-DA analysis was first conducted on faeces, and it demonstrated marked metabolic distinctions between the SAENA, NSAE, and SH groups (Fig. 3A). Using the screening criteria of VIP >1 and $p < 0.05$, we detected 104 significantly differentially abundant metabolites between the SAENA and NSAE groups (Fig. 3B), with 21 metabolites upregulated and 83 downregulated in abundance. Fifty percent of these metabolites were lipids and lipid-like molecules, including PS (20:3(8Z,11Z,14Z)/0:0), PG (20:4(5Z,8Z,11Z,14Z)/0:0), PE (0:0/20:4(8Z,11Z,14Z,17Z)), PC (20:4(8Z,11Z,14Z,17Z)/0:0 and PG (O-20:0/16:0) ($p < 0.05$) (Fig. 3C–G). Through enrichment analysis, enrichment of differentially abundant metabolites was observed in metabolic pathways such as glycerophospholipid metabolism and efferocytosis (Fig. 3H). To characterize overall metabolic differences in rat feces, PLS-DA analysis uncovered significant metabolic variations among the SAENA, SAEA, and SH groups (Fig. 3I). Using the screening criteria of VIP >1 and $p < 0.05$, we detected 589 significantly differentially abundant metabolites between the SAEA and NSAE groups (Fig. 3J), with 277 metabolites upregulated and 312 downregulated in abundance. Differentially abundant metabolites were found to be enriched in autophagy, linoleic acid metabolism and Glycosylphosphatidylinositol (GPI)-anchor biosynthesis pathways via enrichment analysis (Fig. 3K).

Analysis of Metabolites With Different Abundance in the Hippocampus and Associated Pathways

Similarly, PLS-DA based on the hippocampus untargeted metabolomic revealed significant differences in metabolic characteristics among the SAENA, NSAE, and SH groups (Fig. 3L). With the screening thresholds (VIP >1 and $p < 0.05$), we uncovered significantly differentially abundant metabolites in hippocampal tissues among the three groups (Fig. 3M), In the SAE group, the levels of hippocampal metabolites such as PC (15:0/20:5(5Z,8Z,11Z,14Z,17Z)), PE (22:6 (4Z,7Z,10Z,13Z,16Z,19Z)/18:1(11Z)) and PC (20:4(5Z,8Z,11Z,14Z)/P-16:0) were decreased ($p < 0.05$), which showed enrichment in autophagy and glycerophospholipids pathways (Fig. 3N–Q). In addition, PLS-DA based on the hippocampus untargeted metabolomics data revealed significant metabolic differences in the levels of metabolites in the hippocampus among the SAENA, SAEA, and SH groups (Fig. 3R). Using the established thresholds (VIP >1; $p < 0.05$), we detected significantly different metabolites in hippocampal tissues when comparing the SAENA and SAEA groups (Fig. 3S), and these metabolites showed enrichment in glycerophospholipids and autophagy (Fig. 3T). Both in the SAEA and SAENA group, the levels of metabolites related to glycerophospholipid metabolism such as PS (18:0/19:0) and PC (15:0/20:5(5Z,8Z,11Z,14Z,17Z)) and the levels of metabolite associated with autophagy such as PE (22:6(4Z,7Z,10Z,13Z,16Z,19Z)/18:1(11Z)), were all lower than those in the SH group ($p < 0.05$) (Fig. 3U–W). The levels of metabolites of PC (15:0/18:1(11Z)) were decreased in the SAEA group than in the SAENA and SH groups ($p < 0.05$) (Fig. 3X). These data indicate that differentially abundant metabolites in hippocampal tissues were associated with glycerophospholipid metabolism and autophagy in SAE rats.

Integrated analysis of the faecal metabolomics data and hippocampal metabolomics data demonstrated that the differentially abundant metabolites in both the faecal and hippocampal tissues of SAE rats were linked to glycerophospholipid metabolism and the autophagy pathway (Fig. 3Y).

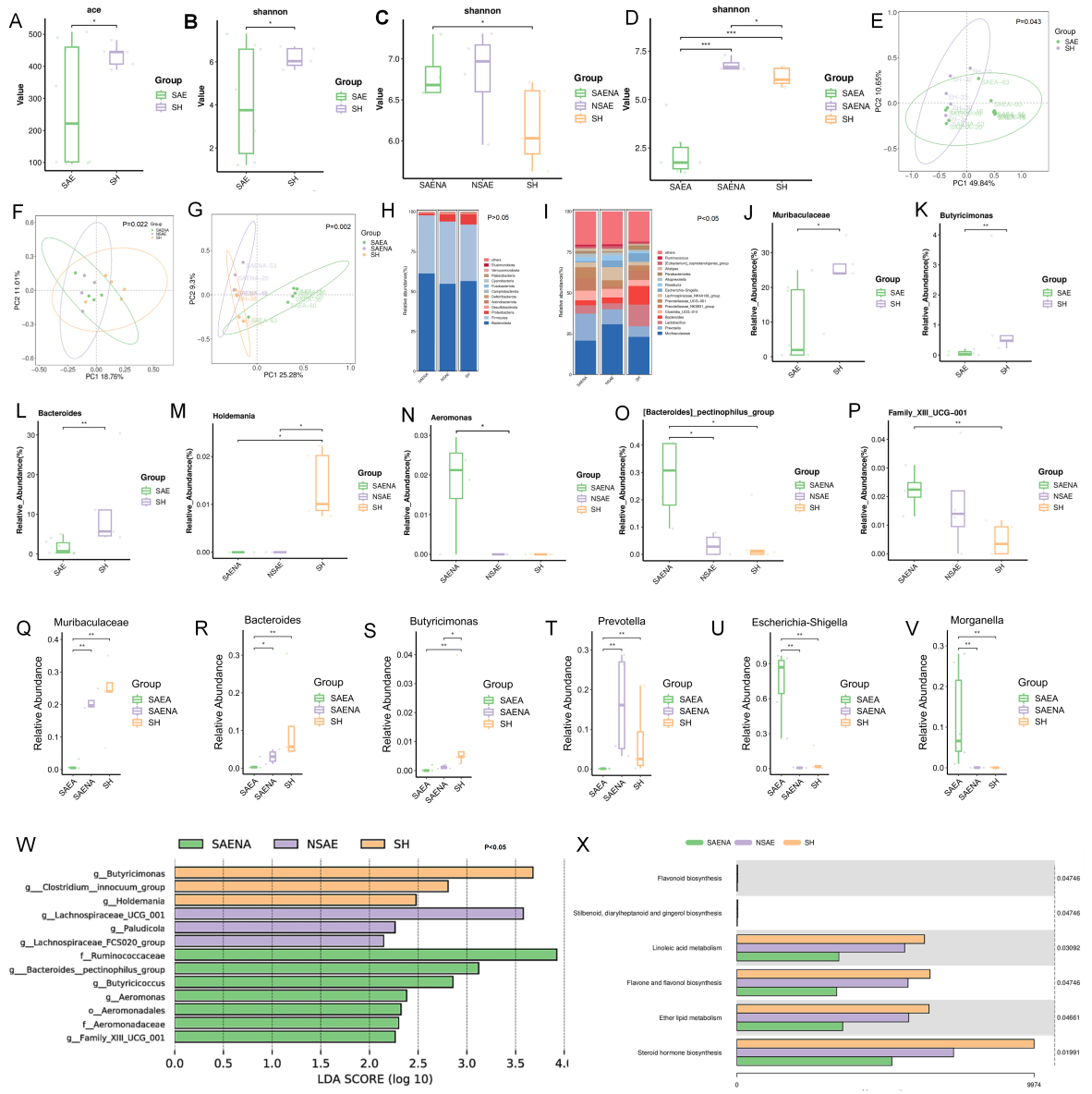

Fig. 2. Variations in the gut microbiota composition caused by sepsis in rats and Metabolic pathway enrichment analysis. (A–D) Alpha-diversity (as assessed by the Shannon index) for the faeces. (E–G) PCA scatterplots of gut microbiota composition data showing the beta diversity for the faeces. (H) The composition of Phylum-level gut microbiota. (I) Genus-level taxonomic profile of gut microbiota. (J–L) The abundances of four bacterial genera significantly differed between the SAE and SH groups at the genus level. (M–P) The abundances of four bacterial genera significantly differed among the SAENA, NSAE and SH groups at the genus level. (Q–V) The abundances of four bacterial genera significantly differed across the SAEA, SAENA and SH groups at the genus level. (W) LEfSe analysis of the gut microbiota and LDA scores. (X) Functional enrichment analysis of metabolic pathways (*$p < 0.05$, **$p < 0.01$, ***$p < 0.001$). n ≥ 4 per group. SAE, sepsis-associated encephalopathy; SH, sham; SAENA, sepsis-associated encephalopathy without antibiotic treatment; NSAE, non-sepsis-associated encephalopathy; SAEA, sepsis-associated encephalopathy with antibiotic treatment; PCA, principal component analysis; LDA, linear discriminant analysis.

Comprehensive Analysis of Differences in the Gut Microbiota and Metabolite Levels in the Gut and Brain

Correlational analysis of differentially abundant metabolite levels in the hippocampus and faeces revealed that the levels of glycerophospholipid metabolism-related metabolites, such as PE (22:6 (4Z, 7Z, 10Z, 13Z, 16Z, 19Z)/18:1 (11Z)), PS (18:0/9:0), and PC (15:0/18:1(11Z)) ($p < 0.05$), in the hippocampus showed positive correlation with the levels of glycerophospholipid metabolism-related metabolites, including PG (20:4(5Z,8Z,11Z,14Z)/0:0), PC(16:0/3:1(2E)), and 1-(2-methoxy-14-methyl-pentadecanyl)-Sn-glycero-3-phosphoserine in the faeces ($p < 0.05$). Thus, in rats

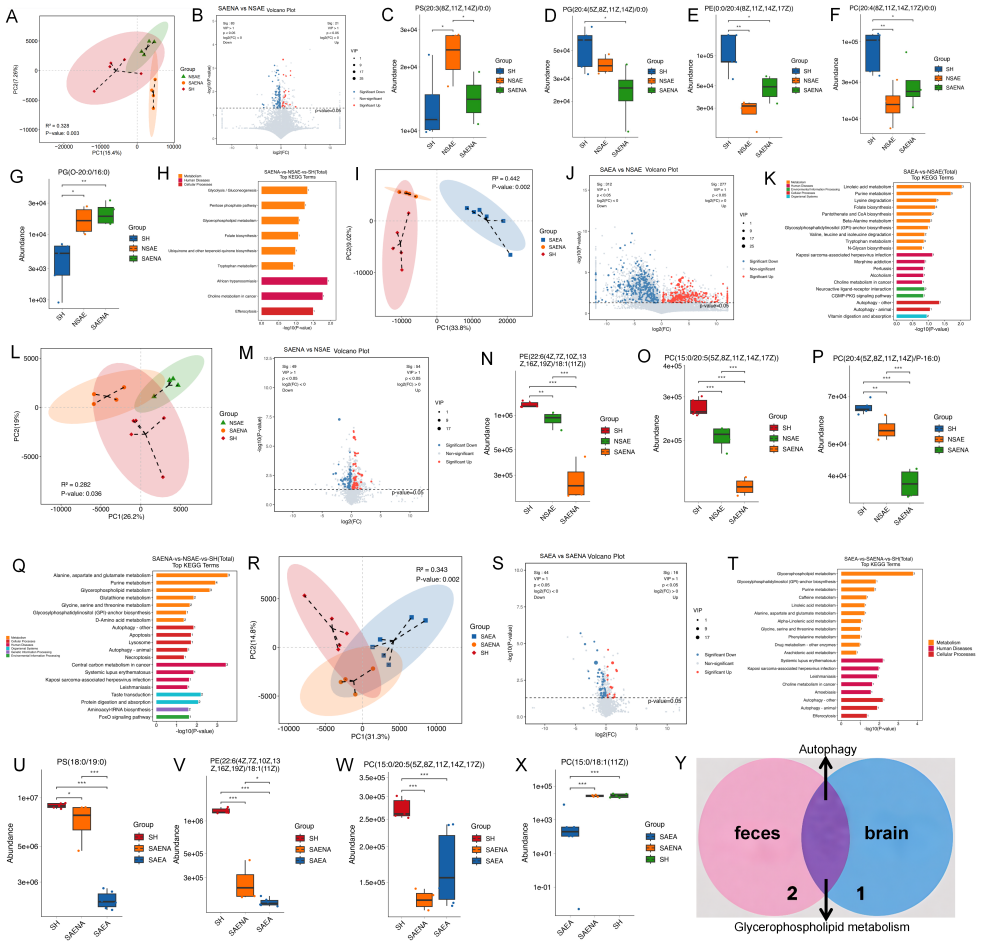

Fig. 3. Differential metabolite levels and enrichment of the top KEGG pathways in both the feces and hippocampus. (A) PLS-DA of metabolite abundance in the faeces among the SAENA, NSAE, and the SH groups. (B) Volcanic map of the differentially abundant metabolites in the feces between different groups (the SAENA and NSAE groups). (C–G) Altered metabolites in the feces among the SAENA, NSAE, and the SH groups. (H) KEGG enrichment analysis of differential metabolites in the feces among the SAENA, NSAE, and the SH groups. (I) PLS-DA of metabolite abundance in the feces among the SAEA, SAENA, and the SH groups. (J) Volcanic map of the differentially abundant metabolites in the feces between different groups (the SAEA and SAENA groups). (K) KEGG enrichment analysis of differential metabolites in the feces among the SAEA, SAENA, and the SH groups. (L) PLS-DA of metabolite abundance in the hippocampus among the SAENA, NSAE, and the SH groups. (M) Volcanic map of the differentially abundant metabolites in the hippocampus between different groups (the SAENA and NSAE groups). (N–P) Altered metabolites in the hippocampus among the SAENA, NSAE, and the SH groups. (Q) KEGG enrichment analysis of differential metabolites in the hippocampus among the SAENA, NSAE, and the SH groups. (R) PLS-DA of metabolite abundance in the hippocampus among the SAEA, SAENA, and the SH groups. (S) Volcanic map of the differentially abundant metabolites in the hippocampus between the SAEA, SAENA, and the SH groups. (T) KEGG enrichment analysis of differential metabolites in the hippocampus among the SAEA, SAENA, and the SH groups. (U–X) Altered metabolites in the hippocampus among the SAEA, SAENA, and the SH groups. (Y) Altered metabolites associated with glycerophospholipid pathways in the feces and hippocampus among different groups. n ≥ 4 per group. *$p < 0.05$, **$p < 0.01$, ***$p < 0.001$). SAENA, sepsis-associated encephalopathy; NSAE, non-sepsis-associated encephalopathy; SAEA, sepsis-associated encephalopathy and antibiotic treatment; SH, sham; KEGG, Kyoto Encyclopedia of Genes and Genomes; PLS-DA, Partial least-squares-discriminant analysis.

with SAE, glycerophospholipid metabolism is a common differentially regulated pathway in the faeces and the brain (Fig. 4A,B).

Next, we further explored the association of abundant gut microbes and the levels of differentially abundant metabolites in the gut. Using correlation analysis, we uncovered significant associations between faecal glycerophospholipid-related metabolites and gut microbial community alterations. The level of the metabolite PG (20:4(5Z,8Z,11Z,14Z)/0:0) in the faeces showed

a positive correlation with the abundance of *Muribaculaceae* (r = 0.81, $p < 0.05$). The level of PC (16:0/3:1(2E)) exhibited a positive association with the abundance of *Butyricimonas* (r = 0.79, $p < 0.05$). The level of 1-(2-Methoxy-14-methyl-pentadecanyl)-Sn-glycero-3-phosphoserine was positively associated with the abundance of the genus *Holdemania* (r = 0.81, $p < 0.05$). The level of PE (0:0/20:4(8Z,11Z,14Z,17Z)) exerted a positive correlation with the abundance of the genus *Holdemania* (r = 0.76, $p < 0.05$) and the abundance of the genus Butyricimonas (r = 0.67, $p < 0.05$). The abundance of Escherichia-Shigella showed a negative correlation with the level of PG (20:4(5Z,8Z,11Z,14Z)/0:0) (r = –0.72, $p < 0.05$) and the level of PC (16:0/3:1(2E)) (r = –0.64, $p < 0.05$) (Fig. 4C,D).

Integrated analysis of multiomics data related to the gut microbiota, faecal metabolites, and brain metabolites revealed that glycerophospholipid metabolism and the autophagy pathway may serve as a critical mediator of gut microbiota-brain crosstalk in SAE rats (Fig. 4E).

Inhibition of the Autophagy Pathway in SAE Rats

Recently, as an important pathway mediating gut microbiota's involvement in SAE progression, autophagy has also attracted wide attention. First, we analyzed the expression of specific proteins and mRNAs related to the autophagy pathway in the hippocampus using Western blot and qRT–PCR analyses. The protein levels of LC3II/LC3I and p-mTOR, as well as the mRNA levels of Beclin 1 and ATG5 in the hippocampus, were significantly reduced in the SAENA group compared to the SH groups ($p < 0.05$) (Fig. 5A–E). Similarly, the protein level of p-mTOR and the mRNA levels of Beclin 1 and ATG5 in the hippocampus were decreased in the SAEA group compared to the SH groups ($p < 0.05$) (Fig. 5D,E). Compared with the SH group, the NSAE group showed statistically significantly higher mRNA levels of ATG5 ($p < 0.05$) (Fig. 5E). Additionally, the NSAE group exhibited higher protein expression of LC3II/LC3I and p-mTOR, as well as higher mRNA levels of Beclin 1, but these differences were not statistically significant ($p > 0.05$) (Fig. 5A–D). Therefore, the hippocampus's autophagy pathway was inhibited in both the SAENA and the SAEA groups. In contrast, the autophagic pathway may be activated in the NSAE group.

Increased Inflammatory Response, and Changes in Apoptotic Pathway in SAE Rats

Furthermore, we analysed the expression of specific proteins and mRNA related to the inflammatory response and the apoptotic pathway in the hippocampus using Western blotting and qRT–PCR analyses. Significant differences in IL-6 protein and mRNA levels were detected in the SAENA group compared to the SH groups ($p < 0.05$) (Fig. 6A–C), indicating a high level of inflammatory cytokine IL-6. Analysis of apoptosis-related indicators revealed no significant differences across all experimental groups. Although Bax/Bcl-2 protein expression and Caspase-3 mRNA levels in the SAENA group were slightly higher than those in the SH group, this change lacked statistical significance, suggesting the absence of notable apoptotic differences among the groups ($p > 0.05$) (Fig. 6D–F).

Discussion

Several studies have demonstrated that the bidirectional gut-brain communication significantly contributes to the pathogenesis and progression of SAE [26,27]. However, owing to the intestinal barrier and BBB, the influence of intestinal microbes on the GBA is indirect rather than direct, and the precise molecular mechanisms remain incompletely characterized. In this study, we identified characteristic variations in the gut microbiota, faecal metabolism, hippocampal metabolism, and cerebral autophagic pathways in a SAE rat model. Our results indicate that gut microbiota may contribute to SAE pathogenesis through regulation of glycerophospholipid metabolism and cerebral autophagic pathways.

In this study, we quantified neurological function in the SAE rat models with a validated scoring scale and EEG. Consistent with the results of other studies [28], a neurological score <6 points 24 hours after LPS injection combined with CLP served as a rapid and effective indicator of SAE. In this study, the incidence rate of SAE was 45.6%, the SAENA group exhibited substantially lower survival, with 33.3% survival at 24 hours and 28% survival at 3 days. In contrast, the NSAE group and SAEA group demonstrated markedly higher survival than the SAENA group. Additionally, the use of neurological scores combined with EEG improved the accuracy of diagnosing SAE, as confirmed by hippocampal and cortical histopathology. In addition, we also found that some septic rats exhibited diarrhea, which is a manifestation of gut dysbiosis.

Gut microbiota dysbiosis is common in septic mouse models and septic patients [28–31]. We identified a differential genus-level abundance of gut microbiota between SAE rats and NSAE rats, including decreased abundances of Bacteroides, Muribaculaceae, Butyricimonas and Holdemania and increased abundances of Aeromonas, Family_XIII_UCG-001. Significant variations were observed in both the diversity and species richness of the gut microbial community. Distinct from the above results, a recent study compared the gut microbiota of mice with severe SAE and mild SAE, and no significant difference was observed in gut microbiota diversity indices [23]. Although the previous study has identified no significant differences in gut microbiota diversity indices between mild and severe SAE mice, another study has shown that the relative abundance of Alloprevotella, Muribaculaceae and Prevotella_9 decreased in the sepsis rats [29], which aligns with our findings. Previous studies have

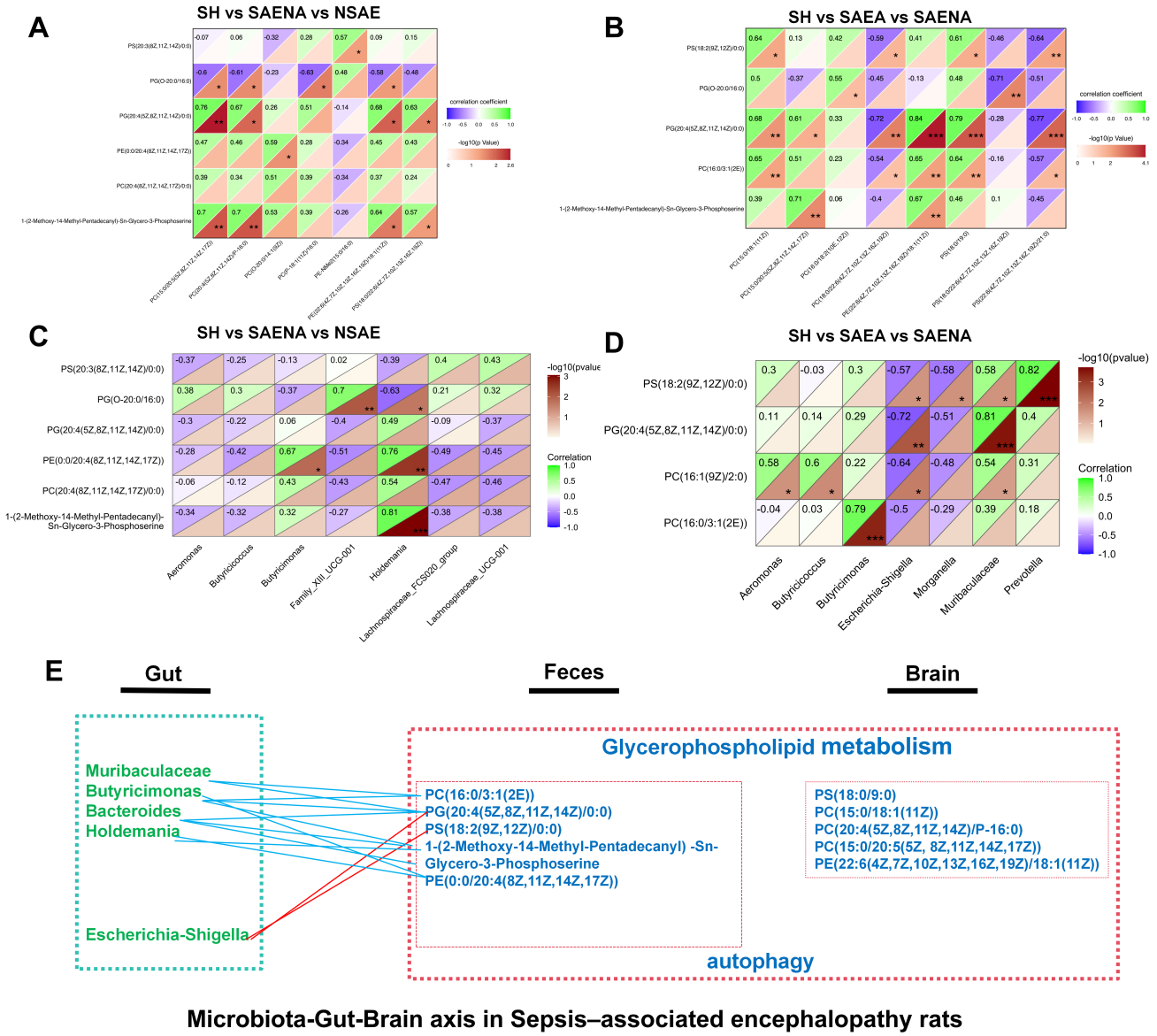

Microbiota-Gut-Brain axis in Sepsis–associated encephalopathy rats

Fig. 4. Correlation analysis of differential gut microbes and metabolites in faeces and brain tissue. (A,B) Correlation analysis of the levels of differentially abundant metabolites in the faeces and hippocampus. (C,D) Spearman correlation analysis between differential gut microbes and metabolites in feces. (E) Network analysis displaying associations between differential gut microbes and metabolites in feces and hippocampus. Negative and positive correlations are indicated by blue and red edges, respectively. $*p < 0.05$, $**p < 0.01$, $***p < 0.001$, n ≥ 4 per group, SAENA, sepsis-associated encephalopathy; NSAE, non-sepsis-associated encephalopathy; SAEA, sepsis-associated encephalopathy combed with antibiotic treatment; SH, sham.

demonstrated that the Firmicutes (Bacillota)/Bacteroidota (F/B) ratio and the abundance of the Lachnospiraceae NK4A136 group were decreased in murine sepsis models, and these alterations were positively correlated with perturbations in 5′-methylthioadenosine, curdione, and PC (18:3(9Z,12Z,15Z)/18:0), which collectively contributed to hippocampal dysfunction [30]. This is consistent with our findings, indicating a potential association between gut dysbiosis and the pathogenesis of sepsis-associated encephalopathy (SAE). Furthermore, our findings indicate that modulating the gut microbiota represents a promising therapeutic strategy for SAE. Moreover, alterations in the gut microbiota were significantly correlated with disturbances in glycerophospholipid metabolism.

Accumulating evidence indicates that SAE is related to changes in multiple endogenous metabolites [31]. Glycerophospholipids, including phosphatidylcholine and phosphatidylethanolamine, serve as fundamental membrane components and are essential for maintaining cellular integrity and physiological function [32]. Glycerophospholipids (GPLs) play a critical role in regulating cellular apoptosis through the modulation of intracellular signalling

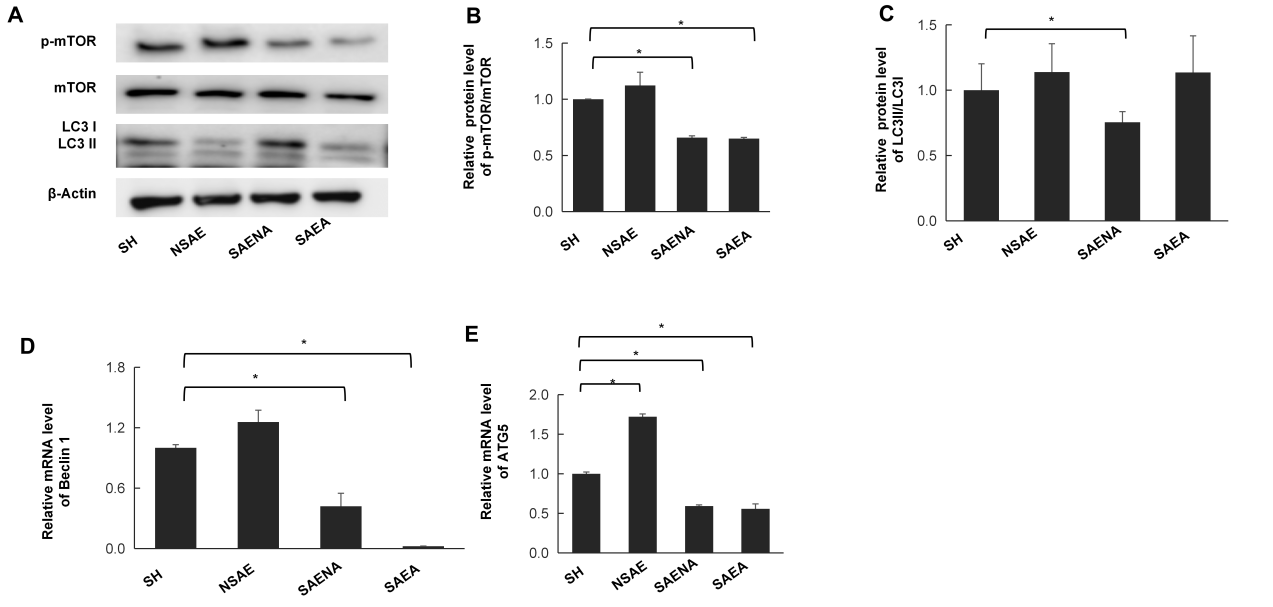

Fig. 5. Differential expression of autophagy in hippocampus. (A–C) Western blotting showing LC3-II, LC3-I, and p-mTOR, mTOR levels and quantitative analysis of LC3-II and LC3-I levels. (D) The mRNA levels of Beclin-1 measured by PCR. (E) The mRNA levels of ATG5 measured by PCR. All experiments were conducted with three independent replicates. n = 3 per group. *$p < 0.05$. SAENA, sepsis-associated encephalopathy; NSAE, Non-sepsis-associated encephalopathy, SAEA, Sepsis-associated encephalopathy with antibiotics, SH, sham group.

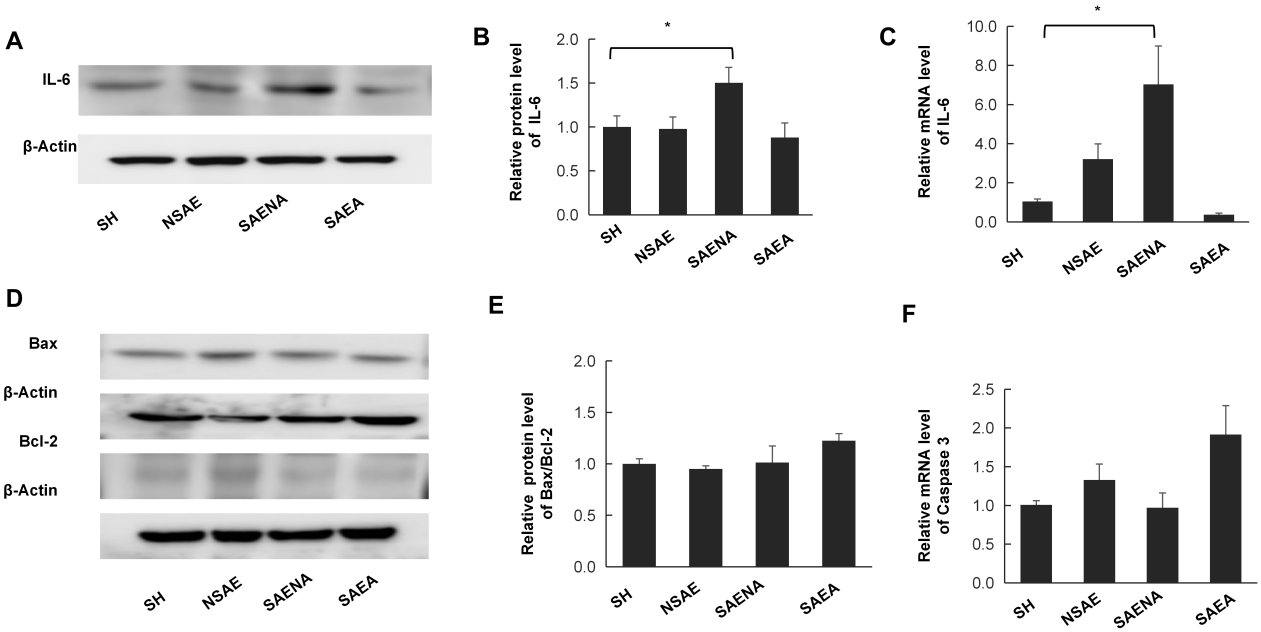

Fig. 6. Differential expression of inflammation and apoptosis markers in hippocampus. (A) IL-6 expression assessed by Western blotting and PCR. (B,C) IL-6 mRNA levels measured by PCR. (D,E) The relative protein levels of Bax and Bcl-2 assessed by Western blotting. (F) Caspase-3 mRNA levels measured. All experiments were conducted with three independent replicates; n = 3 per group. *$p < 0.05$. SAENA, sepsis-associated encephalopathy; NSAE, Non-sepsis-associated encephalopathy, SAEA, Sepsis-associated encephalopathy with antibiotics, SH, sham group.

pathways, epigenetic mechanisms, and membrane transport processes [32,33]. However, a cohort study in sepsis patients demonstrated that levels of phosphatidylcholine (PC) and phosphatidylethanolamine (PE) in both plasma

and cerebrospinal fluid were significantly lower in patients with SAE compared to those without SAE [34]. In SAE mice, PS exerts anti-neuroinflammatory effects by targeting the BK1/NLRP3/ASC signalling pathway and modulating the structure of the gut microbiota [35]. Furthermore, several studies shown that alterations in glycerophospholipid metabolism are linked to the gut microbiota-brain axis both in traumatic brain injury mice and depression mice models [36–39]. Similar to the above research results, we observed a significant reduction in both hippocampal differential metabolites and faeces metabolites associated with glycerophospholipid metabolism in SAE rats. Furthermore, antibiotic treatment could regulate glycerophospholipid metabolism in SAE. which indicates that glycerophospholipid metabolism was associated with the gut microbiota-brain axis in SAE. We speculate that dysregulation of glycerophospholipid metabolism may represent a potential early pathogenic event in the development of SAE and may promote the development of SAE.

Recent studies have confirmed that crosstalk between autophagy and neuroinflammation is closely associated with SAE [40–42]. Similar to the previous report, our results showed that differential hippocampal and faeces metabolites were all enriched in the autophagy pathway in SAE rats, with diminished expression of autophagy-related metabolites in this model. These findings were further validated using WB and PCR analyses, which also demonstrated hippocampal autophagy biomarkers' downregulation, including LC3II/LC3I as well as Beclin 1 and ATG5, and notable perturbations in the expression of hippocampal inflammatory markers. However, since all tissue samples in this study were collected at Day 3 (D3) post-treatment, p-mTOR expression exhibited a trend suggestive of autophagy activation, whereas notable differences were detected between the SH group and the SAENA/SAEA groups. We hypothesize that this conflicting observation is most likely associated with the D3 sampling time window, which may have captured a transient, time-specific state of the autophagic signalling pathway rather than a stable, definitive regulatory pattern.

Similarly, several studies have shown that hippocampal autophagy is downregulated in SAE rat models and that promoting autophagy can alleviate cognitive impairment in these models [41,42]. Our findings corroborate the existing evidence from previous studies. Furthermore, a number of studies indicate that the gut microbiota and autophagy interact in a bidirectional manner. Defective autophagy promotes the development of gut dysbiosis; conversely, gut dysbiosis can drive the development of defective autophagy [43,44]. This study identifies glycerophospholipid metabolism as a key mediator, connecting the gut microbiota with defective autophagy and subsequent neuroinflammation in SAE. Recent studies have indicated that glycerophospholipid metabolism is a potential mediator of systemic immunity and inflammation [45]. Nevertheless, the mechanism by which glycerophospholipid metabolism in the host regulates CNS inflammation has yet to be fully elucidated and warrants further exploration.

The potential limitations of this study should not be ignored. First, to elucidate the involvement of the gut microbiota and glycerophospholipid metabolism in the pathogenesis of SAE more accurately, we used molecular biology methods such as Western blotting and qRT–PCR for validation; further genetic techniques, such as metagenomics and metaproteomics, may be required to explore the underlying mechanisms for more exact identification. Second, only observational experiments were conducted in this study, and experiments involving interventions, such as microbiota transplantation, were not performed to validate the current conclusions. Therefore, further experiments involving cellular experiments and microbiota transplantation are needed for additional verification. Third, this is a preclinical study conducted solely in animal models, and future research involving clinical samples is necessary to confirm these experimental results.

Conclusions

In summary, by integrating multi-omics data, we comprehensively profiled a triad of concurrent alterations in SAE rats: altered gut microbiota, decreased glycerophospholipid metabolism in both the faeces and brain, decreased autophagy metabolism in the brain, and inhibition of activity of hippocampal autophagic pathways by WB and PCR analyses. Furthermore, associations among the gut microbiota, glycerophospholipid metabolism, and reduced autophagy in SAE rats may exist. Our results can promote understanding of the crosstalk between intestinal flora and glycerophospholipid metabolism in SAE rats, which provides evidence for the pathogenesis of SAE and offers new insights for therapeutic targets for SAE.

Abbreviations

SAE, Sepsis-associated encephalopathy; SAENA, sepsis-associated encephalopathy without antibiotic treatment; NSAE, Non Sepsis-associated encephalopathy; SH, Sham; SAEA, Sepsis-associated encephalopathy with antibiotics; LPS, lipopolysaccharide; CLP, caecal ligation and puncture; BBB, blood-brain barrier; CNS, central nervous system; SCFAs, short-chain fatty acids; GBA, Gut-Brain Axis; EEG, electroencephalographic; vEEG, video-electroencephalogram; HE, Haematoxylin–eosin; PCA, principal component analysis; PLS-DA, Partial least-squares-discriminant analysis; VIP, Variable importance of projection; OPLS-DA, orthogonal partial least-squares-discriminant analysis; LDA, linear discriminant analysis.

Availability of Data and Materials

All data generated or analyzed in this study are included in this published article and its accompanying supplementary information.

Author Contributions

WW and WZ: conception, design and critical revision of the article; YL: conception and design; YL, ZQ, AZ, QH, QQ: acquisition of data, analysis and interpretation of data; HL, YZ, and QZ contributed to analysis and interpretation of data; YL, ZQ, AZ, QH, QQ, HL, YZ, QZ: drafting the manuscript; YL, QZ, AZ, QH : review and critical editing; WW: Acquisition of funding. All authors made a significant contribution to the work reported. All authors have given final approval of the version to be published and agreed to be accountable for all aspects of the work in ensuring that questions related to the accuracy or integrity of any part of the work are appropriately investigated and resolved.

Ethics Approval and Consent to Participate

All experimental procedures were approved by the Animal Ethics Committee of The Second Hospital of Hebei Medical University and performed in accordance with institutional guidelines (ethics number: 2023–AE322). All surgeries were performed under anesthesia, and efforts were undertaken to minimize animal's pain, suffering, and death.

Acknowledgment

Special gratitude is extended to Academician Chunyan Li of the Neurology Key Laboratory (The Second Hospital of Hebei Medical University) for facilitating this research through equipment and technical support.

Funding

This work was funded by the Hebei Provincial Department of Health (NO. 20180310) and the National Natural Science Foundation of China (81671292).

Conflict of Interest

The authors declare no conflict of interest.

Supplementary Material

Supplementary material associated with this article can be found, in the online version, at https://doi.org/10.24976/Discov.Med.202638206.72.

References

[1] Singer M, Deutschman CS, Seymour CW, Shankar-Hari M, Annane D, Bauer M, *et al*. The Third International Consensus Definitions for Sepsis and Septic Shock (Sepsis-3). JAMA. 2016; 315: 801–810. https://doi.org/10.1001/jama.2016.0287.

[2] Huang M, Cai S, Su J. The Pathogenesis of Sepsis and Potential Therapeutic Targets. International Journal of Molecular Sciences. 2019; 20: 5376. https://doi.org/10.3390/ijms20215376.

[3] Carter BL, Underwood J. Sepsis and the brain: a review for acute and general physicians. Clinical Medicine (London, England). 2022; 22: 392–395. https://doi.org/10.7861/clinmed.2022-0346.

[4] Gofton TE, Young GB. Sepsis-associated encephalopathy. Nature Reviews. Neurology. 2012; 8: 557–566. https://doi.org/10.1038/nrneurol.2012.183.

[5] Gareau MG. The Microbiota-Gut-Brain Axis in Sepsis-Associated Encephalopathy. MSystems. 2022; 7: e0053322. https://doi.org/10.1128/msystems.00533-22.

[6] Yin XY, Tang XH, Wang SX, Zhao YC, Jia M, Yang JJ, *et al*. HMGB1 mediates synaptic loss and cognitive impairment in an animal model of sepsis-associated encephalopathy. Journal of Neuroinflammation. 2023; 20: 69. https://doi.org/10.1186/s12974-023-02756-3.

[7] Ferreira FM, Gomes SV, Carvalho LCF, de Alcantara AC, da Cruz Castro ML, Perucci LO, *et al*. Potential of piperine for neuroprotection in sepsis-associated encephalopathy. Life Sciences. 2024; 337: 122353. https://doi.org/10.1016/j.lfs.2023.122353.

[8] Haileselassie B, Joshi AU, Minhas PS, Mukherjee R, Andreasson KI, Mochly-Rosen D. Mitochondrial dysfunction mediated through dynamin-related protein 1 (Drp1) propagates impairment in blood brain barrier in septic encephalopathy. Journal of Neuroinflammation. 2020; 17: 36. https://doi.org/10.1186/s12974-019-1689-8.

[9] Xie Z, Xu M, Xie J, Liu T, Xu X, Gao W, *et al*. Inhibition of Ferroptosis Attenuates Glutamate Excitotoxicity and Nuclear Autophagy in a CLP Septic Mouse Model. Shock (Augusta, Ga.). 2022; 57: 694–702. https://doi.org/10.1097/SHK.0000000000001893.

[10] Wang H, Xu L, Tang X, Jiang Z, Feng X. Lipid peroxidation-induced ferroptosis as a therapeutic target for mitigating neuronal injury and inflammation in sepsis-associated encephalopathy: insights into the hippocampal PEBP-1/15-LOX/GPX4 pathway. Lipids in Health and Disease. 2024; 23: 128. https://doi.org/10.1186/s12944-024-02116-x.

[11] Sun J, Fleishman JS, Liu X, Wang H, Huo L. Targeting novel regulated cell death: Ferroptosis, pyroptosis, and autophagy in sepsis-associated encephalopathy. Biomedicine & Pharmacotherapy. 2024; 174: 116453. https://doi.org/10.1016/j.biopha.2024.116453.

[12] Zhu DD, Huang YL, Guo SY, Li N, Yang XW, Sui AR, *et al*. AQP4 Aggravates Cognitive Impairment in Sepsis-Associated Encephalopathy through Inhibiting Na_v 1.6-Mediated Astrocyte Autophagy. Advanced Science (Weinheim, Baden-Wurttemberg, Germany). 2023; 10: e2205862. https://doi.org/10.1002/advs.202205862.

[13] Mittal R, Coopersmith CM. Redefining the gut as the motor of critical illness. Trends in Molecular Medicine. 2014; 20: 214–223. https://doi.org/10.1016/j.molmed.2013.08.004.

[14] Ahmed H, Leyrolle Q, Koistinen V, Kärkkäinen O, Layé S, Delzenne N, *et al*. Microbiota-derived metabolites as drivers of gut-brain communication. Gut Microbes. 2022; 14: 2102878. https://doi.org/10.1080/19490976.2022.2102878.

[15] Wozniak H, Beckmann TS, Fröhlich L, Soccorsi T, Le Terrier C, de Watteville A, *et al*. The central and biodynamic role of gut microbiota in critically ill patients. Critical Care

(London, England). 2022; 26: 250. https://doi.org/10.1186/s13054-022-04127-5.

[16] Sorboni SG, Moghaddam HS, Jafarzadeh-Esfehani R, Soleimanpour S. A Comprehensive Review on the Role of the Gut Microbiome in Human Neurological Disorders. Clinical Microbiology Reviews. 2022; 35: e0033820. https://doi.org/10.1128/CMR.00338-20.

[17] Needham BD, Kaddurah-Daouk R, Mazmanian SK. Gut microbial molecules in behavioural and neurodegenerative conditions. Nature Reviews. Neuroscience. 2020; 21: 717–731. https://doi.org/10.1038/s41583-020-00381-0.

[18] Wang Q, Yang Q, Liu X. The microbiota-gut-brain axis and neurodevelopmental disorders. Protein & Cell. 2023; 14: 762–775. https://doi.org/10.1093/procel/pwad026.

[19] Hu Y, Wang Z, Pan S, Zhang H, Fang M, Jiang H, *et al*. Melatonin protects against blood-brain barrier damage by inhibiting the TLR4/ NF-κB signaling pathway after LPS treatment in neonatal rats. Oncotarget. 2017; 8: 31638–31654. https://doi.org/10.18632/oncotarget.15780.

[20] Peng X, Luo Z, He S, Zhang L, Li Y. Blood-Brain Barrier Disruption by Lipopolysaccharide and Sepsis-Associated Encephalopathy. Frontiers in Cellular and Infection Microbiology. 2021; 11: 768108. https://doi.org/10.3389/fcimb.2021.768108.

[21] Liu T, Li J, Liu Y, Xiao N, Suo H, Xie K, *et al*. Short-chain fatty acids suppress lipopolysaccharide-induced production of nitric oxide and proinflammatory cytokines through inhibition of NF-κB pathway in RAW264.7 cells. Inflammation. 2012; 35: 1676–1684. https://doi.org/10.1007/s10753-012-9484-z.

[22] Erny D, Hrabě de Angelis AL, Jaitin D, Wieghofer P, Staszewski O, David E, *et al*. Host microbiota constantly control maturation and function of microglia in the CNS. Nature Neuroscience. 2015; 18: 965–977. https://doi.org/10.1038/nn.4030.

[23] Fang H, Wang Y, Deng J, Zhang H, Wu Q, He L, *et al*. Sepsis-Induced Gut Dysbiosis Mediates the Susceptibility to Sepsis-Associated Encephalopathy in Mice. MSystems. 2022; 7: e0139921. https://doi.org/10.1128/msystems.01399-21.

[24] Wang X, Wen X, Yuan S, Zhang J. Gut-brain axis in the pathogenesis of sepsis-associated encephalopathy. Neurobiol Dis. 2024;195:106499. https://doi.org/10.1016/j.nbd.2024.106499.

[25] Siami S, Annane D, Sharshar T. The encephalopathy in sepsis. Critical Care Clinics. 2008; 24: 67–82, viii. https://doi.org/10.1016/j.ccc.2007.10.001.

[26] Maramattom BV. Sepsis associated encephalopathy. Neurological Research. 2007; 29: 643–646. https://doi.org/10.1179/016164107X240233.

[27] Alves-Filho JC, de Freitas A, Russo M, Cunha FQ. Toll-like receptor 4 signaling leads to neutrophil migration impairment in polymicrobial sepsis. Critical Care Medicine. 2006; 34: 461–470. https://doi.org/10.1097/01.ccm.0000198527.71819.e1.

[28] Kafa IM, Bakirci S, Uysal M, Kurt MA. Alterations in the brain electrical activity in a rat model of sepsis-associated encephalopathy. Brain Research. 2010; 1354: 217–226. https://doi.org/10.1016/j.brainres.2010.07.049.

[29] Zhao H, Lyu Y, Zhai R, Sun G, Ding X. Metformin Mitigates Sepsis-Related Neuroinflammation *via* Modulating Gut Microbiota and Metabolites. Frontiers in Immunology. 2022; 13: 797312. https://doi.org/10.3389/fimmu.2022.797312.

[30] Song F, Li Q, Cui J, Wang J, Xiao S, Yu B, *et al*. Exploring the gut microbiota-hippocampus-metabolites axis dysregulation in sepsis mice. Frontiers in Microbiology. 2024; 15: 1302907. https://doi.org/10.3389/fmicb.2024.1302907.

[31] Liu J, Jin Y, Li H, Yu J, Gong T, Gao X, *et al*. Probiotics Exert Protective Effect against Sepsis-Induced Cognitive Impairment by Reversing Gut Microbiota Abnormalities. Journal of Agricultural and Food Chemistry. 2020; 68: 14874–14883. https://doi.org/10.1021/acs.jafc.0c06332.

[32] Guido ME, Monjes NM, Wagner PM, Salvador GA. Circadian Regulation and Clock-Controlled Mechanisms of Glycerophospholipid Metabolism from Neuronal Cells and Tissues to Fibroblasts. Molecular Neurobiology. 2022; 59: 326–353. https://doi.org/10.1007/s12035-021-02595-4.

[33] Fiume R, Faenza I, Sheth B, Poli A, Vidalle MC, Mazzetti C, *et al*. Nuclear Phosphoinositides: Their Regulation and Roles in Nuclear Functions. International Journal of Molecular Sciences. 2019; 20: 2991. https://doi.org/10.3390/ijms20122991.

[34] Qin M, Yu S, Lu X, Gong C, Song Z, Zhu H, *et al*. Reduced phosphatidylcholine and phosphatidylethanolamine levels correlate with inflammatory activation in sepsis-associated encephalopathy. European Journal of Medical Research. 2025; 30: 828. https://doi.org/10.1186/s40001-025-03115-z.

[35] Xu K, Huang Q, Lyu Y, Wang S, Lu Y, Qian G. Phosphatidylserine improves aging sepsis survival, modulates gut microbiome, and prevents sepsis-associated encephalopathy. Biomedicine & Pharmacotherapy. 2024; 178: 117200. https://doi.org/10.1016/j.biopha.2024.117200.

[36] Sarkar C, Lipinski MM. Glycerophospholipid dysregulation after traumatic brain injury. Neurochemistry International. 2024; 175: 105701. https://doi.org/10.1016/j.neuint.2024.105701.

[37] Zheng P, Wu J, Zhang H, Perry SW, Yin B, Tan X, *et al*. The gut microbiome modulates gut-brain axis glycerophospholipid metabolism in a region-specific manner in a nonhuman primate model of depression. Molecular Psychiatry. 2021; 26: 2380–2392. https://doi.org/10.1038/s41380-020-0744-2.

[38] Tian T, Mao Q, Xie J, Wang Y, Shao WH, Zhong Q, *et al*. Multi-omics data reveals the disturbance of glycerophospholipid metabolism caused by disordered gut microbiota in depressed mice. Journal of Advanced Research. 2022; 39: 135–145. https://doi.org/10.1016/j.jare.2021.10.002.

[39] Xie J, Zhong Q, Wu WT, Chen JJ. Multi-omics data reveals the important role of glycerophospholipid metabolism in the crosstalk between gut and brain in depression. Journal of Translational Medicine. 2023; 21: 93. https://doi.org/10.1186/s12967-023-03942-w.

[40] Li Y, Wang F, Luo Y. Ginsenoside Rg1 protects against sepsis-associated encephalopathy through beclin 1-independent autophagy in mice. The Journal of Surgical Research. 2017; 207: 181–189. https://doi.org/10.1016/j.jss.2016.08.080.

[41] Du L, Wu Y, Jia Q, Li J, Li Y, Ma H, *et al*. Autophagy Suppresses Ferroptosis by Degrading TFR1 to Alleviate Cognitive Dysfunction in Mice with SAE. Cellular and Molecular Neurobiology. 2023; 43: 3605–3622. https://doi.org/10.1007/s10571-023-01370-4.

[42] Liu W, Guo J, Mu J, Tian L, Zhou D. Rapamycin Protects Sepsis-Induced Cognitive Impairment in Mouse Hippocampus by Enhancing Autophagy. Cellular and Molecular Neurobiology. 2017; 37: 1195–1205. https://doi.org/10.1007/s10571-016-0449-x.

[43] Saint-Georges-Chaumet Y, Edeas M. Microbiota-mitochondria inter-talk: consequence for microbiota-host interaction. Pathogens and Disease. 2016; 74: ftv096. https://doi.org/10.1093/femspd/ftv096.

[44] Chidambaram SB, Essa MM, Rathipriya AG, Bishir M, Ray B, Mahalakshmi AM, *et al*. Gut dysbiosis, defective autophagy and altered immune responses in neurodegenerative diseases: Tales of a vicious cycle. Pharmacology & Therapeutics. 2022; 231: 107988. https://doi.org/10.1016/j.pharmthera.2021.107988.

[45] Kan Y, Wang H, Lin H, Li Y, Pei S, Cui Y, *et al*. Transcript and Lipid Profile Alterations in Astrocyte-Neuron Mitochondrial Transfer Under Lipopolysaccharide Exposure: An In Vitro Study. Journal of Neurochemistry. 2025; 169: e70003. https://doi.org/10.1111/jnc.70003.